NANO LETTERS

pubs.acs.org/NanoLett Letter

Actin Architecture Steers Microtubules in Active Cytoskeletal Composite

Ondřej Kučera,* Jérémie Gaillard, Christophe Guérin, Clothilde Utzschneider, Manuel Théry,* and Laurent Blanchoin*

Cite This: https://doi.org/10.1021/acs.nanolett.2c03117 Read Online

ACCESS | Metrics & More | Article Recommendations | Supporting Information

ABSTRACT: Motility assays use surface-immobilized molecular motors to propel cytoskeletal filaments. They have been widely used to characterize motor properties and their impact on cytoskeletal self-organization. Moreover, the motility assays are a promising class of bioinspired active tools for nanotechnological applications. While these assays involve controlling the filament direction and speed, either as a sensory readout or a functional feature, designing a subtle control embedded in the assay is an ongoing challenge. Here, we investigate the interaction between gliding microtubules and networks of actin filaments. We demonstrate that the microtubule's behavior depends on the actin architecture. Both unbranched and branched actin decelerate microtubule gliding; however, an unbranched actin network provides additional guidance and effectively steers the microtubules. This effect, which resembles the recognition of cortical actin by microtubules, is a conceptually new means of controlling the filament gliding with potential application in the design of active materials and cytoskeletal nanodevices.

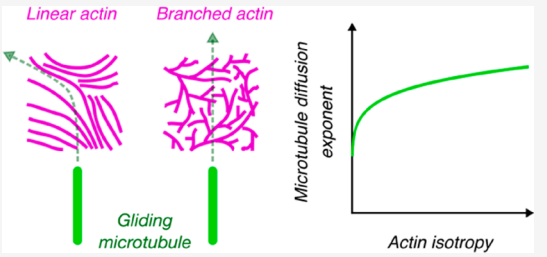

KEYWORDS: *microtubules, actin filaments, gliding assay, network architecture, cytoskeletal composite*

Microtubules and actin filaments are biopolymers that form the cytoskeleton in eukaryotic cells. Through their dissipative self-assembly, crosstalk, interaction with motor proteins and a plethora of regulatory factors, these cytoskeletal structures underlie fundamental biological processes such as transport, motility, and morphogenesis.[1,2] The building blocks of the cytoskeletal machinery can be, thanks to their self-organizing properties, isolated from cells and reconstructed into functional assemblies *in vitro*. Transcending the original purpose of the reconstitution biology, i.e. reducing the complexity of biological machinery under controlled conditions, the *in vitro* cytoskeletal experimentation has led to the development of active materials[3] and nanodevices for sensory applications or nonclassical computing.[4−7] A great portion of artificial cytoskeletal systems makes use of gliding assay. In this assay, cytoskeletal filaments are propelled along a surface by ATP-consuming motor proteins grafted onto this very surface. An application of the gliding assay involves regulation of the filament gliding, either as a sensory readout or a functional feature. It can be achieved by the modulation of the motor activity[8−10] or by steering the gliding direction by geometrical constraints[11−16] and external forces.[17−20]

An interesting opportunity to regulate the filament gliding stems from the interaction of filaments with themselves, the underpinning of collective phenomena,[3] by the assistance of molecular linkers[21−26] or depletion forces.[27,28] Although the main focus has been on single species of biopolymers, either microtubules or actin filaments, recent works inspired by cytoskeletal crosstalk in cells[2] have shown that combining the cytoskeletal components in a composite[29] brings additional qualities to gliding assays.[30−32] Nevertheless, the main qualitative property of cytoskeletal crosstalk, its dependence on the actin architecture,[2] remained unexplored.

Here, we scrutinize the interaction landscape between motile microtubules and the two types of actin architecture: linear actin filaments or branched actin network (by the Arp2/3 complex).[33] To this end, we developed a microtubule gliding assay in the presence of actin filaments. In this system, we observed that actin filaments influence the behavior of microtubules by imposing friction and providing guidance cues by alignment. Notably, the microtubule gliding was directionally controlled by actin architecture and its anisotropic structural geometry. This effect, which is reminiscent of recognizing cortical actin architecture by microtubules in cells,[2,33] can be exploited to design active materials and cytoskeletal nanodevices.

Received: August 5, 2022
Revised: October 18, 2022

https://doi.org/10.1021/acs.nanolett.2c03117
Nano Lett. XXXX, XXX, XXX−XXX

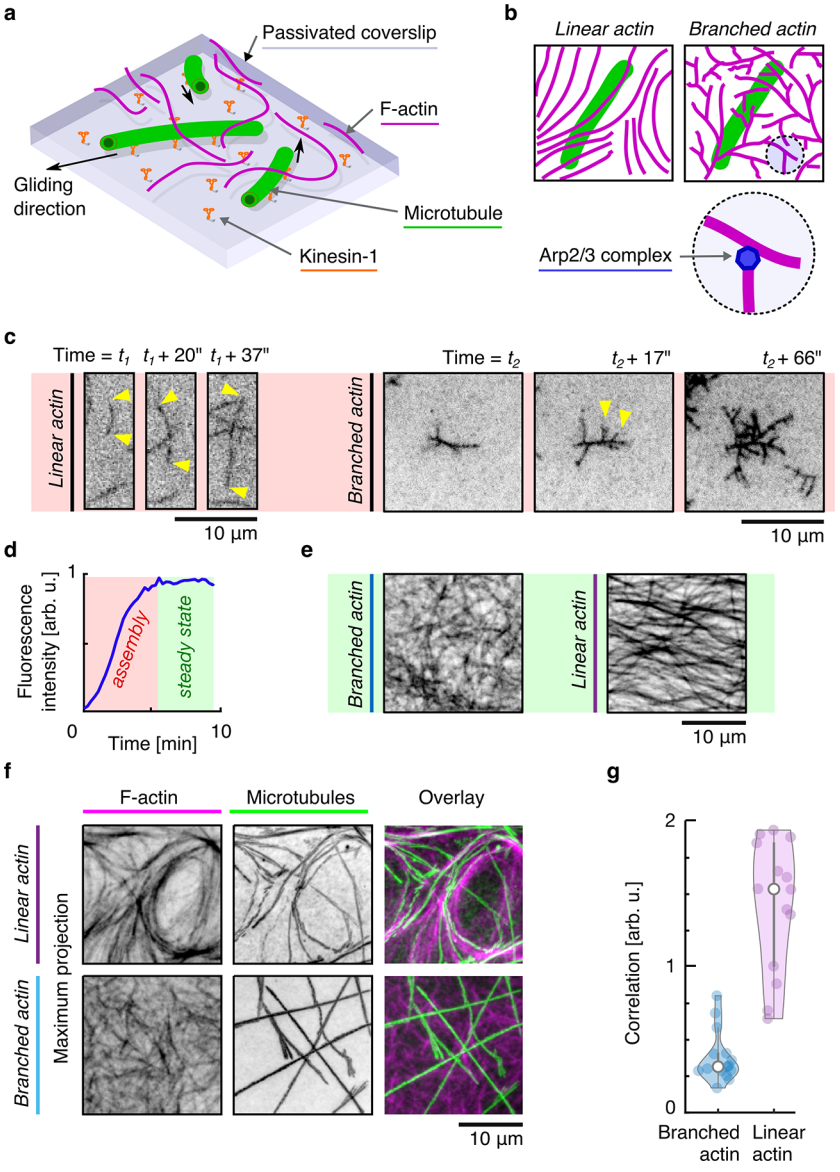

Figure 1. Microtubule gliding assay in the presence of actin networks. (a) Schematic representation of the assay. (b) Schematic representation of a microtubule in linear and branched actin network. (c) Time-lapse intensity inverted fluorescence micrographs of polymerization of linear actin and branched actin filaments. The yellow arrowheads indicate the ends of the filament (linear actin) and newly grown branches (branched actin). (d) The temporal profile of actin fluorescence intensity reveals the polymerization state of actin filaments (a typical example). (e) Intensity inverted fluorescence micrographs of branched and linear actin networks in the saturation condition. (f) Maximum projection images of actin networks and microtubules reveal the microtubule guidance by linear actin. (g) Correlation of maximum projections of corresponding actin and microtubule images ($N = \nu = 14$ and 15 per condition, $n = 3$). Individual data points are accompanied by violin plots: Central marks represent the median, top and bottom edges of the box indicate the 75th and 25th percentiles, respectively. Whiskers extend the 95% confidence intervals.

We attached kinesin-I motors to a glass surface at the density of 17.4 μm^{-2} and let them propel prepolymerized GMPCPP microtubules in the presence of linear actin architecture, or a branched network (using the Arp2/3 complex, Figure 1a,b, Supporting Methods). Microtubules were introduced at a low concentration reducing the probability of their collisions during gliding, which would otherwise dominate the system's behavior (Figure S1). The untethered actin mesh was polymerized *in situ* using a crowding agent (Figure 1c). Using TIRF microscopy imaging, we monitored the growth of the actin and waited until the actin fluorescence intensity reached a plateau when we started the observation of gliding microtubules (Figure 1d). We note that the actin mesh, at this time, is forming a relatively homogeneous "carpet" with a distinctive internal organization given by the actin architecture (Figure 1e). This property of branched actin results from the kinetics of the network polymerization (Figure S2).

We observed that microtubules sense the local organization in the linear actin mesh and use it as a template for their trajectories (Figure 1f). The measurement of the angle between microtubules and the dominant local orientation of actin filaments confirmed that microtubules tend to align with linear actin (median, 8°; 75% percentile, 18°; maximum angle, 89°; $N = 380$, $\nu = 10$, $n = 3$). This effect, which resembles cortical microtubule guidance, was, by contrast, unnoticeable in the branched actin network (Figure 1f). The correlation of maximum temporal projection of microtubule trajectories (projection time 180 s) with the actin geometry (Figure 1g)

https://doi.org/10.1021/acs.nanolett.2c03117
Nano Lett. XXXX, XXX, XXX−XXX

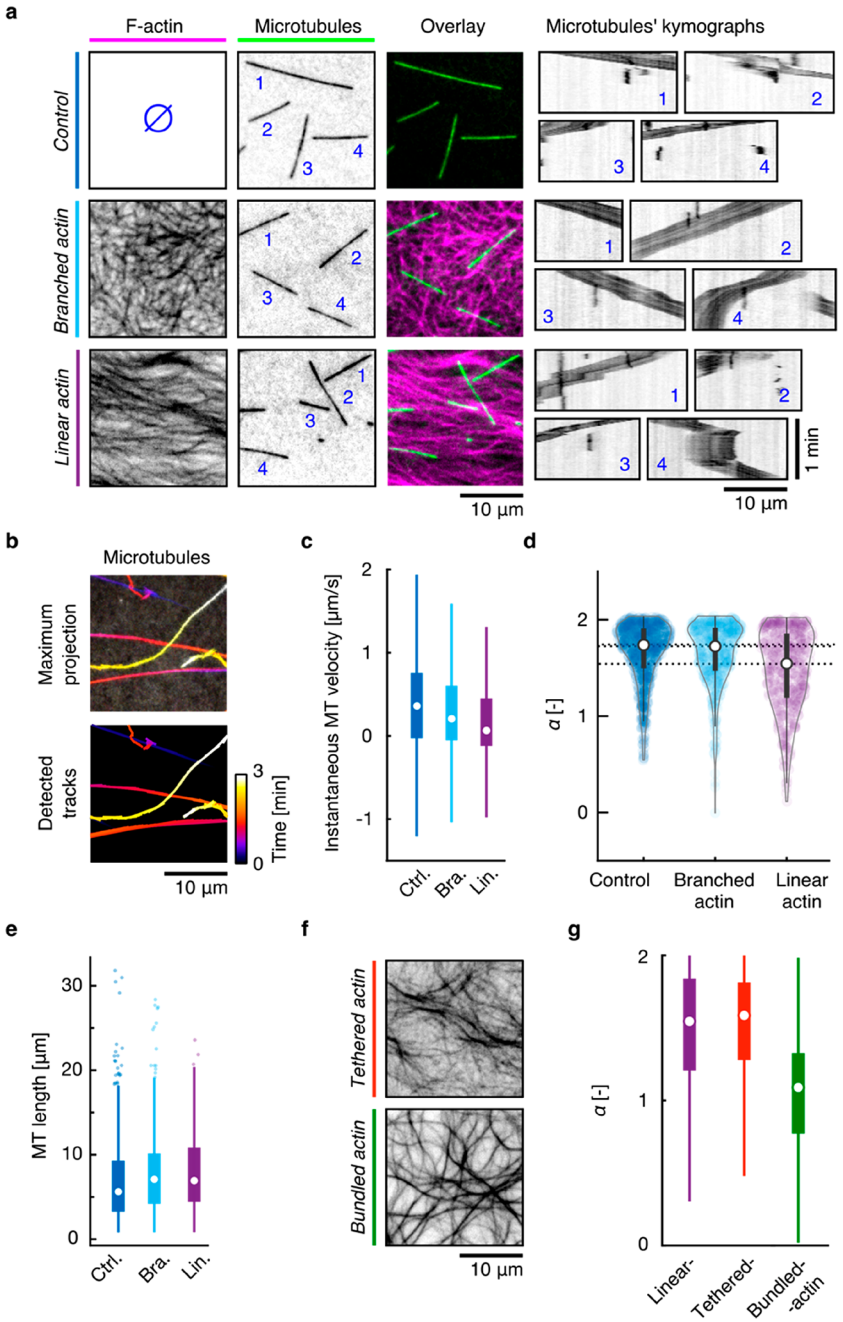

Figure 2. Microtubule motility is controlled by actin architecture. (a) Typical fluorescence micrographs of actin and microtubules with corresponding kymographs of microtubule motility. (b) An example of temporal color-coded maximum projection of microtubule mobility and corresponding detected microtubule tracks. (c) Box plot of instantaneous microtubule velocities (outliers not shown). (d) Diffusion exponent, α, for all detected microtubule tracks (Control: $N = 666$, $\nu = 9$, $n = 3$. Branched actin: $N = 479$, $\nu = 10$, $n = 3$. Linear actin: $N = 380$, $\nu = 10$, $n = 3$). (e) Comparison of detected microtubule lengths in control experiments and in the presence of branched and linear actin. (f) Inverse intensity fluorescence micrographs of tethered and bundled linear actin filaments. (g) The comparison of the diffusion exponent of microtubules gliding in the three types of linear actin (Linear actin: $N = 380$, $\nu = 10$, $n = 3$. Tethered actin: $N = 2452$, $\nu = 7$, $n = 2$. Bundled actin: $N = 114$, $\nu = 21$, $n = 2$.). Central marks represent the median, top and bottom edges of the box indicate the 75th and 25th percentiles, respectively. Whiskers extend the 95% confidence intervals.

confirmed the difference as highly reproducible (Mann–Whitney U-test of equal medians, $p = 9.43 \times 10^{-6}$). Since we did not observe transport or visible deformation of actin by single motile microtubules, we presume that this actin-architecture-specific behavior of motile microtubules stems from a geometry-related difference in the actin microenvironment.

Compared to control in the absence of actin, we observed that the gliding of microtubules in both actin architectures appeared slower (Figure 2a), indicating that the actin network acts as a mechanical resistance. Occasionally, in the presence of actin filaments, microtubules exhibited markedly complex velocity profiles with pausing or quick switching of the gliding direction, leading sporadically to a quasi-oscillatory movement (Figure S3). These observations indicate inhomogeneities,

https://doi.org/10.1021/acs.nanolett.2c03117
Nano Lett. XXXX, XXX, XXX−XXX

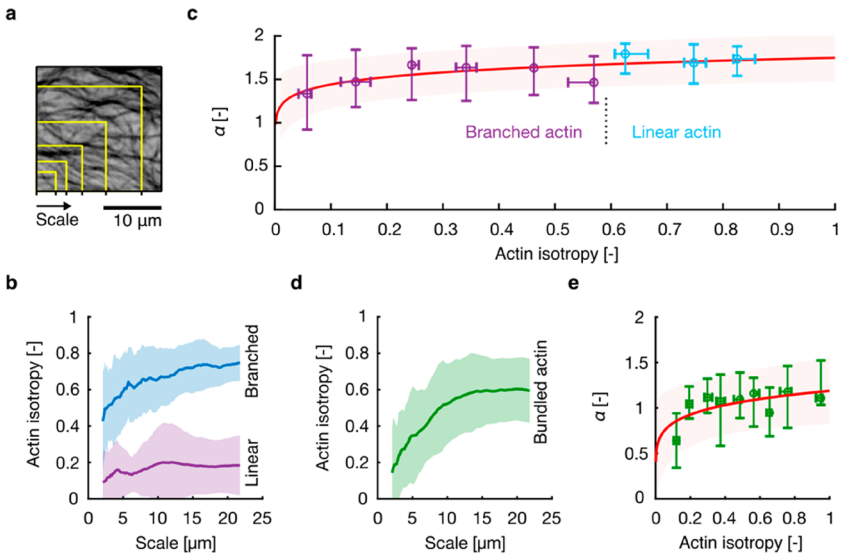

Figure 3. Microtubule motility depends on the isotropy of actin network. (a) Illustration of the concept of scale. (b) Actin isotropy as a function of scale for linear and branched actin. Data are represented as mean (solid line) ± s.d. (shadowed area). Branched actin: $\nu = 10$, $n = 3$. Linear actin: $\nu = 10$, $n = 3$). (c) The diffusion exponent, α, as a function of actin isotropy. Data are binned and represented as median with whiskers extending to lower and upper quartiles. The red curve represents the power-law fit to medians within each bin ($R^2 = 0.6$), and the shadowed area represents the 95% confidence interval. (d) Actin isotropy as a function of scale for bundled actin. Data are represented as mean (solid line) ± s.d. (shadowed area). (e) Diffusion exponent of microtubules gliding in bundled actin vs actin isotropy corresponding to the microtubule length. Central marks indicate median and the error bars indicate 75th and 25th percentiles of the data. The red curve represents the power-law fit ($R^2 = 0.44$) to medians within each bin, and the shadowed area represents the 95% confidence interval. See Figure S6 for the data in panels c and e shown in the logarithmic scale.

nonlinear effects, the presence of elastic coupling between the polymers, or a complex combination of these factors, which will be difficult to fit into a more quantitative picture.

We tracked all microtubules in our assay to quantify the microtubule response to their microenvironment. The information about microtubule position at each time-point of the observation gave us access to microtubule trajectories (Figure 2b) and instantaneous velocities (Figure 2c). Since very short trajectories cannot be reliably analyzed, in the following, we selected only those microtubules that covered a distance of at least 6 μm, which is an experimentally tuned compromise between the spatial-temporal resolution of the image acquisition and the data fitting.

First, using the trajectories, we plot the mean-squared displacement, MSD, of the microtubules (Figure S4a). MSD is coupled with the delay, or the time interval over which it is measured, by a power law, MSD $\propto \tau^{\alpha}$. The value of the diffusion exponent, α, demarcates three regimes of the motion: subdiffusion related to confinement ($0 < \alpha < 1$), random diffusion ($\alpha \approx 1$), and superdiffusion ($1 < \alpha < 2$). By curve fitting, we determined the values of the diffusion exponents from our experimental data ($R^2 = 0.98$, $N = 1525$ microtubule trajectories). The comparison of the distributions of the diffusion exponent (Figure 2d) revealed that the values measured in all groups predominantly correspond to super-diffusive motion ($1 < \alpha < 2$), in concordance with the visual inspection of the microtubules' motions.

The values of α under control condition, i.e. microtubules gliding in the absence of actin (α = 1.74:1.51−1.89 (median: 25th quartile−75th quartile), $N = 666$, $\nu = 9$, $n = 3$) and in the presence of branched actin (α = 1.72:1.49−1.90, $N = 479$, $\nu = 10$, $n = 3$) were not different (Mann−Whitney U-test of equal medians, $p = 0.71$). In the linear actin, however, was the diffusion exponent (α = 1.55:1.21−1.84, $N = 380$, $\nu = 10$, $n = 3$) significantly reduced compared to control ($p = 1.55 \times 10^{-11}$). Increasing the motor surface density above a factor of 1.5 led to the diminishing of this effect (Figure S4b). Microtubules longer than 10 μm, which in each group represent approximately 25% of microtubules (Figure 2e), tend to evince larger α (1.87, 1.84, and 1.75 (median) for the control condition, branched actin, and linear actin, respectively) compared to shorter microtubules (1.72, 1.68, and 1.46) (Figure S4c). Microtubules with diffusive and sub-diffusive trajectories ($\alpha \leq 1$) were almost three times more likely to be found in linear actin than in the other two groups (14% vs 5% of the corresponding populations), indicating increased confinement. Tethering the actin filaments partially to the substrate by the biotin-neutravidin link (Supporting Information) did not change this behavior (Figure 2f,g), providing a piece of strong evidence that the variation in the strength of the actin depletion from the volume of the channel is not the cause of the observed difference. Bundling the filaments by α-actinin (a cross-linker that promotes the formation of actin bundles), in contrast, leads to a strong decrease in the diffusion exponent (Figure 2f,g), indicating that the architectural features of the actin network, which practically determine the interaction landscape experienced by microtubules, are the key parameter controlling the trajectories. We assume that the reduction of actin flexibility and the local augmentation of the interaction surface, both resulting from actin bundling, are responsible for this observed decrease in the diffusion exponent

To link these results to the actin architecture, we first quantified the geometrical organization of actin. Isotropic parameter analysis (Supporting Information) confirmed that the branched network is highly isotropic, unlike the linear actin. There is virtually no overlap of the isotropic parameter value between the two architectures regardless of the scale over

https://doi.org/10.1021/acs.nanolett.2c03117
Nano Lett. XXXX, XXX, XXX−XXX

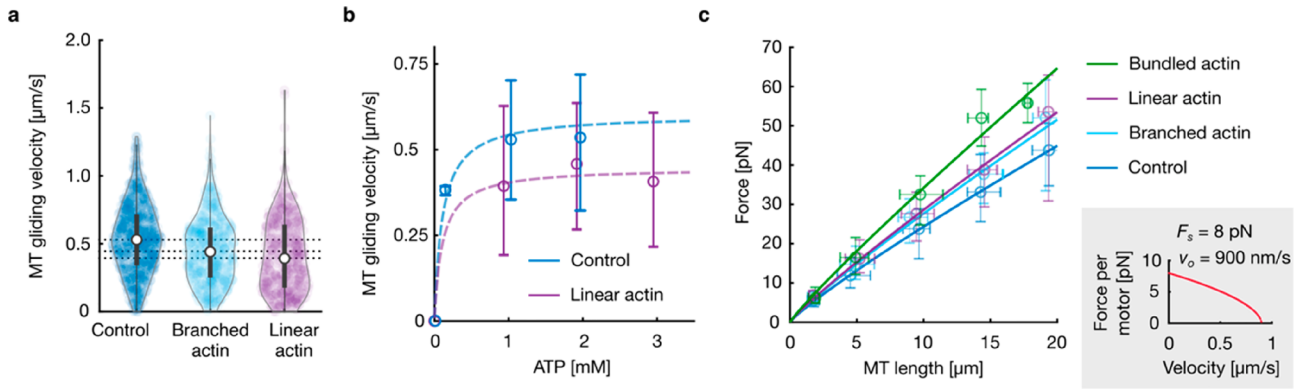

Figure 4. Analysis of the friction between actin filaments and microtubules. (a) Violin plots of the velocities of microtubules gliding in the absence of actin and in the linear and branched actin networks. Individual data points are accompanied by violin plots: Central marks represent the median, top and bottom edges of the box indicate the 75th and 25th percentiles, respectively. Whiskers extend the 95% confidence intervals. (b) Microtubule gliding velocity as a function of ATP concentration. Data are represented as median, and whiskers extend to lower and upper quartiles. The dashed lines represent the rough estimates of Michaelis–Menten model (see the main text). (c) The force opposing microtubule movement as a function of microtubule length. Data are binned and represented as median with whiskers extending to lower and upper quartiles. Solid line plots are fits to the binned data. The force–velocity model used for the force estimation is shown in the inset.

which it is measured (Figure 3a,b). Nevertheless, the spread of the values of the isotropic parameter from several replicates led us to couple the microtubule diffusion exponents to the isotropic parameters of actin in which they were observed. A plot of these coupled values revealed a functional relation between the actin isotropy and the diffusion coefficient of microtubules gliding in this actin organization (Figure 3c). Regardless of the actin architecture, the higher actin isotropy leads, on average, to a higher diffusion exponent of microtubules, following an empirical power-law increase.

We tested this observation further by repeating the same analysis in the linear actin network bundled by α-actinin. On a large uniform scale, contrary to our previous observations, we did not observe a clear functional relation (Figure S5). However, we note that the bundled network has dramatically altered isotropy, which is strongly dependent on the scale because the mesh size of the network is relatively large (Figure 3d). Once we corrected the scale of the actin isotropy to the scale of each microtubule, practically adjusting the scale to the size of the microenvironment experienced by the microtubule, the clear functional pattern reappeared (Figure 3e).

Having shown that microtubules sense and respond to actin architecture, we aimed to scrutinize the effect of the actin microenvironment on the gliding velocity of microtubules. Tracking the microtubules revealed that their mean gliding velocity has a rather wide distribution and is, on average, lower in the presence of actin (0.4 μm·s^{-1} (median) in both architectures) than at control condition without actin (0.5 μm·s^{-1}) (Figure 4a), confirming the initial visual observations (Figure 2a). Increasing the concentration of ATP did not lead to an increase in the gliding velocity, demonstrating that the experiments were performed at the saturation condition[34] and confirming thus that the lower velocity in the presence of actin is not an experimental artifact stemming from inconsistencies in ATP concentration (Figure 4b). The difference between rough estimates of Michaelis–Menten velocity data fits (assuming that the Michaelis constant, which is lower than 0.88 mM with 95% empirical probability, is not affected by the presence of actin) suggests that the interaction of microtubules with actin is asymptotically responsible for a 26% reduction of the median gliding velocity (13% combined uncertainty). If the force–velocity curve of gliding microtubules were linear, this reduction would indicate that the friction force would, on average, reach 26% of the force required to stall the microtubule.

The viscous drag, as well as the friction, are both functions of the microtubule length. As the samples of microtubules at the three conditions have similar yet not precisely identical lengths (Figure 2 e), we next decoupled the distributions. We estimated the forces opposing microtubule gliding based on the three-parameter model of the force–velocity relation[35,36] from the average gliding velocity, $\overline{v}$, as $F = F_S \frac{L}{\langle d \rangle}\left(1 - \frac{\overline{v}}{v_o}\right)^{1/w}$, where F_S is the stall force of the motor, L is the length of the microtubule, $\langle d \rangle$ is the average distance between microtubule-attached motors, v_o is the velocity of the unloaded motor, and w is a scaling parameter.[36] For the calculations, the following values of the parameters were used: F_S = 8 pN, $\langle d \rangle$ = 1.8 μm, v_o = 0.9 μm s^{-1}, and w = 1.8.[37] In all groups, the opposing force increases with the microtubule length (Figure 4c). The control group exhibited a substantial, slightly nonlinear trend with viscous drag from the medium and friction with the substrate as the assumed main contributing factors. We interpret the additive force in the presence of actin networks, which has a linear trend (R^2 > 0.97 for all groups) since the majority of observed velocities fall within the linear part of the force–velocity curve, as the friction force between actin filaments and the microtubule. The addition is, per unit of microtubule length, 0.33 pN·μm^{-1} (95% confidence interval, 0.15–0.52 pN·μm^{-1}) in branched and 0.43 pN·μm^{-1} (95% confidence interval, 0.25–0.60 pN·μm^{-1}) in linear actin. We compacted linear actin with α-actinin to investigate this additive opposing force further. Doing so increased the opposing force by a factor of 2 per unit length of a microtubule compared to linear actin alone, providing evidence that the opposing forces are of frictional character.

We have studied the response of microtubules propelled by molecular motors to the presence of different actin architectures. Complementary to previous reports that focused on emergent collective effects in the cytoskeletal composite with a minimum information on the behavior of single microtubules,[30,31] here we analyzed the interaction of

https://doi.org/10.1021/acs.nanolett.2c03117
Nano Lett. XXXX, XXX, XXX–XXX

individual microtubules with actin filaments. Since the lengths of microtubules had a similar distribution in all the experimental groups reported here, and the length-decoupled data retained systematic differences, we can conclude that the observed differences between the groups were solely due to the actin architecture. Within the groups, shorter microtubules, which are associated with fewer surface-bound kinesin-1 motors, were more sensitive to the presence of actin. The torsional compliance of kinesin motors provides enhanced rotational freedom to microtubules which are tethered to a very small number of motors.[38,39] External cues can, therefore, deflect the trajectory of the short microtubule more easily than that of long microtubules, where additional force is required to deform the microtubule lattice. Along the same lines, the motor surface density is an important parameter influencing the sensitivity of microtubules in the gliding assay. Lower motor density enables microtubule tips to explore a larger area by thermal fluctuations and, at the same time, it limits the ability of microtubules to overcome hindering forces, even though this relationship is not linear.[36] Our observation that the increase of the motor density suppresses the effect of actin on the diffusion exponent of microtubules agrees well with this established understanding of the sensitivity of the gliding assay. We speculate that incorporating kinesin motors into the lipid bilayer, which regulates the force that motors can effectively produce by enabling their lateral diffusivity,[40−42] could be instrumental for the further development of our assay. It would also allow for patterning both types of actin architectures simultaneously.

Our results show that the most dramatic effects of actin on microtubules, the guidance and frictional deceleration, were observed in an anisotropic unbranched actin network, which enables tight alignment between the cytoskeletal polymers. This level of alignment could not be achieved in a branched actin network, where the microtubule is equally likely to encounter actin filament in any direction, making the mechanical environment and the interaction landscape highly isotropic. To observe some alignment, the distance between branching nodes would have to become comparable with the size of a microtubule or higher. Even though such a condition is experimentally inaccessible without changing the density of the actin network, the experiment with bundled actin network, which practically delivers a larger mesh size, confirms this view.

The absence of transport or visible deformation of actin filaments by motile microtubules indicates that if they become physically blocked by actin, microtubules cannot surpass the viscous drag of the medium on the actin network with which they interact. Such situations are predominantly transient as the microtubules can change their gliding direction. The intriguing, nevertheless, rare observation of quasi-oscillatory microtubule movement indicates elastic coupling[43] to actin by local strains in the actin mesh.[44] In the future, direct force measurements shall help resolve this question in greater detail. Generally, the dominant forces hindering the microtubule movement are friction[45] and compaction.[46] Friction has recently been established as an important factor in the behavior of active materials.[47] In our assay, the friction has various components, and we estimated the additive contribution caused by the presence of actin filaments. While the friction between cytoskeletal filaments is generally assumed to be nonlinear,[45] this friction in our assay has a fairly linear character due to the limited width of the velocities population, which largely falls within the linear regime of the force−velocity model used.[35−37] The compaction, which is caused by the presence of methylcellulose, is essential to (i) offset the electrostatic repulsion between microtubules and actin filaments and (ii) stabilize the actin mesh at the coverslip surface. Although we could not vary the concentration of methylcellulose in our experiments due to the use of untethered actin filaments, we can assume that the variation of the depletant concentration would modulate the strength of the interaction, similarly to other experiments with cytoskeletal polymers.[27] Both friction and compaction depend on the geometry of the interacting surfaces and, thus, on the actin architecture in our experiments. The possibility of tight alignment between microtubules and linear actin architecture shall maximize the compaction and frictional forces, and our observations agree with this assumption.

Here, we dissected the interaction of low-density single microtubules with actin mesh. Increasing the microtubule surface density led to the prevalence of microtubule-microtubule interactions, which translated into microtubule ordering (Figure S1). This self-organization was manifestly reinforced by linear actin, similarly to our earlier report,[31] while the effect of the branched actin network was indistinct (Figure S1).

The recognition of actin architecture by microtubules in mammalian cell cortex is governed by the microtubule dynamics,[48,49] cross-linking[50,51] and retrograde actin flow,[52−54] which, in contrast to our assay, result in negligible movement of microtubule lattice relative to actin network.[55,56] Nevertheless, our findings highlight the importance of the effects that nonspecific steric interactions may have in biological or bioinspired systems.[46,57]

While the interaction between linear actin filaments and microtubules in gliding assays has been studied recently with main focus on emerging collective effects,[30,31] here we demonstrate that the actin architecture regulates the gliding of microtubules up to direct steering. We foresee a large potential for employing these findings in active materials and nanodevices, especially with patterned actin architectures, or in systems supporting dynamic switch of the actin architecture from linear to branched and *vice versa*. Since gliding assays have recently transcended beyond cytoskeletal biopolymers,[58] the possibility of controlling the gliding properties by the anisotropy of the soft polymer layer becomes even more controllable and thus better applicable.

■ ASSOCIATED CONTENT

Supporting Information

The Supporting Information is available free of charge at https://pubs.acs.org/doi/10.1021/acs.nanolett.2c03117.

Supporting methods containing methodological details for all parts of the manuscript; supporting references; supplementary Figures S1−S6 containing information as follows: the behavior of the system at high microtubule densities (Figure S1), the architecture of branched actin network at different concentrations of Arp2/3 complex and nucleation promoting factors (Figure S2), complex motility of microtubules in linear actin (Figure S3), additional results of microtubule tracking (Figure S4), the diffusion exponent of microtubules gliding in bundled actin vs maximum scale actin isotropy (Figure S5), and logarithmic scale plot of the diffusion exponent as a function of actin isotropy (Figure S6) (PDF)

https://doi.org/10.1021/acs.nanolett.2c03117
Nano Lett. XXXX, XXX, XXX−XXX

AUTHOR INFORMATION

Corresponding Authors

Ondřej Kučera − *CytoMorpho Lab, Laboratoire de Physiologie Cellulaire et Végétale, Interdisciplinary Research Institute of Grenoble, CEA/CNRS/Université Grenoble Alpes, Grenoble 38 054, France;* Present Address: South East Technological University, Cork Road, Waterford, X91 K0EK, Ireland; orcid.org/0000-0002-9559-1717; Email: ondrej.kucera@biophysics.cz

Manuel Théry − *CytoMorpho Lab, Laboratoire de Physiologie Cellulaire et Végétale, Interdisciplinary Research Institute of Grenoble, CEA/CNRS/Université Grenoble Alpes, Grenoble 38 054, France; CytoMorpho Lab, Unité de Thérapie Cellulaire, Hôpital Saint Louis/CNRS/CEA, Paris 75 010, France*; Email: manuel.thery@cea.fr

Laurent Blanchoin − *CytoMorpho Lab, Laboratoire de Physiologie Cellulaire et Végétale, Interdisciplinary Research Institute of Grenoble, CEA/CNRS/Université Grenoble Alpes, Grenoble 38 054, France; CytoMorpho Lab, Unité de Thérapie Cellulaire, Hôpital Saint Louis/CNRS/CEA, Paris 75 010, France*; Email: laurent.blanchoin@cea.fr

Authors

Jérémie Gaillard − *CytoMorpho Lab, Laboratoire de Physiologie Cellulaire et Végétale, Interdisciplinary Research Institute of Grenoble, CEA/CNRS/Université Grenoble Alpes, Grenoble 38 054, France*

Christophe Guérin − *CytoMorpho Lab, Laboratoire de Physiologie Cellulaire et Végétale, Interdisciplinary Research Institute of Grenoble, CEA/CNRS/Université Grenoble Alpes, Grenoble 38 054, France*

Clothilde Utzschneider − *CytoMorpho Lab, Laboratoire de Physiologie Cellulaire et Végétale, Interdisciplinary Research Institute of Grenoble, CEA/CNRS/Université Grenoble Alpes, Grenoble 38 054, France*

Complete contact information is available at: https://pubs.acs.org/10.1021/acs.nanolett.2c03117

Author Contributions

Conceptualization, L.B., M.T., O.K.; methodology, O.K., J.G., C.G.; investigation, O.K., J.G., C.U.; formal analysis, O.K., J.G.; data curation, O.K.; validation, O.K.; resources, O.K., J.G., C.G.; writing, O.K.; visualization, O.K.; supervision, M.T., L.B.; funding acquisition, M.T., L.B.

Notes

The authors declare no competing financial interest.

ACKNOWLEDGMENTS

We thank Laura Aradilla Zapata (Saarland University) for her critical comments on our results and Matthieu Gélin for inspiring this research. This work was supported by the European Research Council, Consolidator Grant 771599 (ICEBERG) to M.T. and Advanced Grant 741773 (AAA) to L.B.. O.K. was partially supported by Pole emploi (7820342X). Our imaging platform is supported by the Laboratory of Excellence Grenoble Alliance for Integrated Structural & Cell Biology (LabEX GRAL)(ANR-10-LABX-49-01) and the University Grenoble Alpes graduate school (Ecoles Universitaires de Recherche, CBH-EUR-GS, ANR-17-EURE-0003).

REFERENCES

(1) Misteli, T. The concept of self-organization in cellular architecture. *J. Cell Biol.* **2001**, *155*, 181−185.

(2) Dogterom, M.; Koenderink, G. H. Actin−microtubule crosstalk in cell biology. *Nat. Rev. Mol. Cell Biol.* **2019**, *20*, 38−54.

(3) Needleman, D.; Dogic, Z. Active matter at the interface between materials science and cell biology. *Nat. Rev. Mater.* **2017**, *2*, 17048.

(4) Reuther, C.; Catalano, R.; Salhotra, A.; Vemula, V.; Korten, T.; Diez, S.; MÅnsson, A. Comparison of actin- and microtubule-based motility systems for application in functional nanodevices. *New J. Phys.* **2021**, *23*, 075007.

(5) Saper, G.; Hess, H. Synthetic Systems Powered by Biological Molecular Motors. *Chem. Rev.* **2020**, *120*, 288−309.

(6) Agarwal, A.; Hess, H. Biomolecular motors at the intersection of nanotechnology and polymer science. *Prog. Polym. Sci.* **2010**, *35*, 252−277.

(7) Korten, T.; Månsson, A.; Diez, S. Towards the application of cytoskeletal motor proteins in molecular detection and diagnostic devices. *Curr. Opin. Biotechnol.* **2010**, *21*, 477−488.

(8) Tas, R. P.; Chen, C. Y.; Katrukha, E. A.; Vleugel, M.; Kok, M.; Dogterom, M.; Akhmanova, A.; Kapitein, L. C. Guided by Light: Optical Control of Microtubule Gliding Assays. *Nano Lett.* **2018**, *18*, 7524−7528.

(9) Kumar, K. R. S.; Amrutha, A. S.; Tamaoki, N. Spatiotemporal control of kinesin motor protein by photoswitches enabling selective single microtubule regulations. *Lab Chip.* **2016**, *16*, 4702−4709.

(10) Amrutha, A. S.; Kumar, K. R. S.; Kikukawa, T.; Tamaoki, N. Targeted Activation of Molecular Transportation by Visible Light. *ACS Nano* **2017**, *11*, 12292−12301.

(11) Lin, C. T.; Kao, M. T.; Kurabayashi, K.; Meyhofer, E. Self-contained, biomolecular motor-driven protein sorting and concentrating in an ultrasensitive microfluidic chip. *Nano Lett.* **2008**, *8*, 1041−1046.

(12) Rupp, B.; Nédélec, F. Patterns of molecular motors that guide and sort filaments. *Lab Chip.* **2012**, *12*, 4903−4910.

(13) Reuther, C.; Mittasch, M.; Naganathan, S. R.; Grill, S. W.; Diez, S. Highly-Efficient Guiding of Motile Microtubules on Non-Topographical Motor Patterns. *Nano Lett.* **2017**, *17*, 5699−5705.

(14) Kaneko, T.; Furuta, K.; Oiwa, K.; Shintaku, H.; Kotera, H.; Yokokawa, R. Different motilities of microtubules driven by kinesin-1 and kinesin-14 motors patterned on nanopillars. *Sci. Adv.* **2020**, *6*, eaax7413.

(15) Schroeder, V.; Korten, T.; Linke, H.; Diez, S.; Maximov, I. Dynamic guiding of motor-driven microtubules on electrically heated, smart polymer tracks. *Nano Lett.* **2013**, *13*, 3434−3438.

(16) Ramsey, L.; Schroeder, V.; Van Zalinge, H.; Berndt, M.; Korten, T.; Diez, S.; Nicolau, D. V. Control and gating of kinesin-microtubule motility on electrically heated thermo-chips. *Biomed. Microdevices* **2014**, *16*, 459−463.

(17) Van Den Heuvel, M. G. L.; Butcher, C. T.; Smeets, R. M. M.; Diez, S.; Dekker, C. High rectifying efficiencies of microtubule motility on Kinesin-coated gold nanostructures. *Nano Lett.* **2005**, *5*, 1117−1122.

(18) Van Den Heuvel, M. G. L.; De Graaff, M. P.; Dekker, C. Microtubule curvatures under perpendicular electric forces reveal a low persistence length. *Proc. Natl. Acad. Sci. U.S.A.* **2008**, *105*, 7941−7946.

(19) Van Den Heuvel, M. G. L.; De Graaff, M. P.; Dekker, C. Molecular Sorting by Electrical Steering of Microtubules in Kinesin-Coated Channels. *Science* **2006**, *312*, 910−914.

(20) Kim, T.; Kao, M. T.; Meyhöfer, E.; Hasselbrink, E. F. Biomolecular motor-driven microtubule translocation in the presence of shear flow: Analysis of redirection behaviours. *Nanotechnology* **2007**, *18*, 025101.

(21) Kabir, A. M. R.; Inoue, D.; Kakugo, A.; Sada, K.; Gong, J. P. Active self-organization of microtubules in an inert chamber system. *Polym. J.* **2012**, *44*, 607−611.

https://doi.org/10.1021/acs.nanolett.2c03117
Nano Lett. XXXX, XXX, XXX−XXX

(22) Inoue, D.; Kabir, A. M. R.; Mayama, H.; Gong, J. P.; Sada, K.; Kakugo, A. Growth of ring-shaped microtubule assemblies through stepwise active self-organisation. *Soft Matter* **2013**, *9*, 7061−7068.
(23) Ito, M.; Kabir, A. M. R.; Inoue, D.; Torisawa, T.; Toyoshima, Y.; Sada, K.; Kakugo, A. Formation of ring-shaped microtubule assemblies through active self-organization on dynein. *Polym. J.* **2014**, *46*, 220−225.
(24) Wada, S.; Rashedul Kabir, A. M.; Ito, M.; Inoue, D.; Sada, K.; Kakugo, A. Effect of length and rigidity of microtubules on the size of ring-shaped assemblies obtained through active self-organization. *Soft Matter* **2015**, *11*, 1151−1157.
(25) Keya, J. J.; Suzuki, R.; Kabir, A. M. R.; Inoue, D.; Asanuma, H.; Sada, K.; Hess, H.; Kuzuya, A.; Kakugo, A. DNA-assisted swarm control in a biomolecular motor system. *Nat. Commun.* **2018**, *9*, 4−11.
(26) Keya, J. J.; Kabir, A. M. R.; Inoue, D.; Sada, K.; Hess, H.; Kuzuya, A.; Kakugo, A. Control of swarming of molecular robots. *Sci. Rep.* **2018**, *8*, 1−10.
(27) Inoue, D.; Mahmot, B.; Kabir, A. M. R.; Farhana, T. I.; Tokuraku, K.; Sada, K.; Konagaya, A.; Kakugo, A. Depletion force induced collective motion of microtubules driven by kinesin. *Nanoscale* **2015**, *7*, 18054−18061.
(28) Saito, A.; Farhana, T. I.; Kabir, A. M. R.; Inoue, D.; Konagaya, A.; Sada, K.; Kakugo, A. Understanding the emergence of collective motion of microtubules driven by kinesins: role of concentration of microtubules and depletion force. *RSC Adv.* **2017**, *7*, 13191−13197.
(29) Lorenz, C.; Köster, S. Multiscale architecture: Mechanics of composite cytoskeletal networks. *Biophys. Rev.* **2022**, *3*, 031304.
(30) Farhadi, L.; Fermino Do Rosario, C.; Debold, E. P.; Baskaran, A.; Ross, J. L. Active Self-Organization of Actin-Microtubule Composite Self-Propelled Rods. *Front. Phys.* **2018**, *6*, 1−16.
(31) Kučera, O.; Gaillard, J.; Guerin, C.; Thery, M.; Blanchoin, L. Actin-microtubule dynamic composite forms responsive active matter with memory. *Proc. Natl. Acad. Sci. U.S.A.* **2022**, *119*, e2209522119.
(32) Choi, D. S.; Byun, K. E.; Hong, S. Dual transport systems based on hybrid nanostructures of microtubules and actin filaments. *Small* **2011**, *7*, 1755−1760.
(33) Blanchoin, L.; Boujemaa-Paterski, R.; Sykes, C.; Plastino, J. Actin Dynamics, Architecture, and Mechanics in Cell Motility. *Physiol. Rev.* **2014**, *94*, 235−263.
(34) Porter, M. E.; Scholey, J. M.; Stemple, D. L.; Vigers, G. P.; Vale, R. D.; Sheetz, M. P.; McIntosh, J. R. Characterization of the microtubule movement produced by sea urchin egg kinesin. *J. Biol. Chem.* **1987**, *262*, 2794−2802.
(35) Gagliano, J.; Walb, M.; Blaker, B.; MacOsko, J. C.; Holzwarth, G. Kinesin velocity increases with the number of motors pulling against viscoelastic drag. *Eur. Biophys. J.* **2010**, *39*, 801−813.
(36) Fallesen, T. L.; MacOsko, J. C.; Holzwarth, G. Force-velocity relationship for multiple kinesin motors pulling a magnetic bead. *Eur. Biophys. J.* **2011**, *40*, 1071−1079.
(37) Fallesen, T. L.; MacOsko, J. C.; Holzwarth, G. Measuring the number and spacing of molecular motors propelling a gliding microtubule. *Phys. Rev. E* **2011**, *83*, 011918.
(38) Howard, J.; Hudspeth, A. J.; Vale, R. D. Movement of microtubules by single kinesin molecules. *Nature* **1989**, *342*, 154−158.
(39) Leduc, C.; Ruhnow, F.; Howard, J.; Diez, S. Detection of fractional steps in cargo movement by the collective operation of kinesin-1 motors. *Proc. Natl. Acad. Sci. U. S. A.* **2007**, *104*, 10847−10852.
(40) Grover, R.; Fischer, J.; Schwarz, F. W.; Walter, W. J.; Schwille, P.; Diez, S. Transport efficiency of membrane-anchored kinesin-1 motors depends on motor density and diffusivity. *Proc. Natl. Acad. Sci. U. S. A.* **2016**, *113*, E7185−E7193.
(41) Memarian, F. L.; Lopes, J. D.; Schwarzendahl, F. J.; Athani, M. G.; Sarpangala, N.; Gopinathan, A.; Beller, D. A.; Dasbiswas, K.; Hirst, L. S. Active nematic order and dynamic lane formation of microtubules driven by membrane-bound diffusing motors. *Proc. Natl. Acad. Sci. U. S. A.* **2021**, *118*, 1−10.
(42) Sciortino, A.; Bausch, A. R. Pattern formation and polarity sorting of driven actin filaments on lipid membranes. *Proc. Natl. Acad. Sci. U. S. A.* **2021**, *118*, e2017047118.
(43) Jülicher, F.; Prost, J. Spontaneous oscillations of collective molecular motors. *Phys. Rev. Lett.* **1997**, *78*, 4510−4513.
(44) Scheff, D. R.; Redford, S. A.; Lorpaiboon, C.; Majumdar, S.; Dinner, A. R.; Gardel, M. L. Actin filament alignment causes mechanical hysteresis in cross-linked networks. *Soft Matter* **2021**, *17*, 5499.
(45) Ward, A.; Hilitski, F.; Schwenger, W.; Welch, D.; Lau, A. W. C.; Vitelli, V.; Mahadevan, L.; Dogic, Z. Solid friction between soft filaments. *Nat. Mater.* **2015**, *14*, 583−588.
(46) Braun, M.; Lansky, Z.; Hilitski, F.; Dogic, Z.; Diez, S. Entropic forces drive contraction of cytoskeletal networks. *BioEssays* **2016**, *38*, 474−481.
(47) Thijssen, K.; Khaladj, D. A.; Aghvami, S. A.; Gharbi, M. A.; Fraden, S.; Yeomans, J. M.; Hirst, L. S.; Shendruk, T. N. Submersed micropatterned structures control active nematic flow, topology, and concentration. *Proc. Natl. Acad. Sci. U. S. A.* **2021**, *118*, e2106038118.
(48) Colin, A.; Singaravelu, P.; Théry, M.; Blanchoin, L.; Gueroui, Z. Actin-Network Architecture Regulates Microtubule Dynamics. *Curr. Biol.* **2018**, *28*, 2647.
(49) Janson, M. E.; De Dood, M. E.; Dogterom, M. Dynamic instability of microtubules is regulated by force. *J. Cell Biol.* **2003**, *161*, 1029−1034.
(50) Alkemade, C.; Wierenga, H.; Volkov, V. A.; Lopez, M. P.; Akhmanova, A.; ten Wolde, P. R.; Dogterom, M.; Koenderink, G. H. Cross-linkers at growing microtubule ends generate forces that drive actin transport. *Proc. Natl. Acad. Sci. U.S.A.* **2022**, *119*, e2112799119.
(51) López, M. P.; Huber, F.; Grigoriev, I.; Steinmetz, M. O.; Akhmanova, A.; Koenderink, G. H.; Dogterom, M. *Nat. Commun.* **2014**, *5* (5), 4778.
(52) Akhshi, T. K.; Wernike, D.; Piekny, A. Microtubules and actin crosstalk in cell migration and division. *Cytoskeleton* **2014**, *71*, 1−23.
(53) Geraldo, S.; Gordon-Weeks, P. R. Cytoskeletal dynamics in growth-cone steering. *J. Cell Sci.* **2009**, *122*, 3595−3604.
(54) Coles, C. H.; Bradke, F. Coordinating Neuronal Actin-Microtubule Dynamics. *Curr. Biol.* **2015**, *25*, R677−R691.
(55) Schaefer, A. W.; Kabir, N.; Forscher, P. Filopodia and actin arcs guide the assembly and transport of two populations of microtubules with unique dynamic parameters in neuronal growth cones. *J. Cell Biol.* **2002**, *158*, 139−152.
(56) Rauch, P.; Heine, P.; Goettgens, B.; Käs, J. A. Forces from the rear: Deformed microtubules in neuronal growth cones influence retrograde flow and advancement. *New J. Phys.* **2013**, *15*, 015007.
(57) Ross, J. L. The Dark Matter of Biology. *Biophys. J.* **2016**, *111*, 909−916.
(58) Ibusuki, R.; Morishita, T.; Furuta, A.; Nakayama, S.; Yoshio, M.; Kojima, H.; Oiwa, K.; Furuta, K. Programmable molecular transport achieved by engineering protein motors to move on DNA nanotubes. *Science* **2022**, *375*, 1159−1164.

https://doi.org/10.1021/acs.nanolett.2c03117
Nano Lett. XXXX, XXX, XXX−XXX